

Article

Transport Mechanisms for CO₂-CH₄ Exchange and Safe CO₂ Storage in Hydrate-Bearing Sandstone

Knut Arne Birkedal *, Lars Petter Hauge, Arne Graue and Geir Ersland

Department of Physics and Technology, University of Bergen, 5007 Bergen, Norway;

E-Mails: Lars.Hauge@ift.uib.no (L.P.H.); Arne.Graue@ift.uib.no (A.G.);

Geir.Ersland@ift.uib.no (G.E.)

* Author to whom correspondence should be addressed;

E-Mail: KnutArne.Birkedal@conocophillips.com; Tel.: +47-45473748.

Academic Editor: Richard Coffin

Received: 18 January 2015 / Accepted: 23 April 2015 / Published: 8 May 2015

Abstract: CO₂ injection in hydrate-bearing sediments induces methane (CH₄) production while benefitting from CO₂ storage, as demonstrated in both core and field scale studies. CH₄ hydrates have been formed repeatedly in partially water saturated Bentheim sandstones. Magnetic Resonance Imaging (MRI) and CH₄ consumption from pump logs have been used to verify final CH₄ hydrate saturation. Gas Chromatography (GC) in combination with a Mass Flow Meter was used to quantify CH₄ recovery during CO₂ injection. The overall aim has been to study the impact of CO₂ in fractured and non-fractured samples to determine the performance of CO₂-induced CH₄ hydrate production. Previous efforts focused on diffusion-driven exchange from a fracture volume. This approach was limited by gas dilution, where free and produced CH₄ reduced the CO₂ concentration and subsequent driving force for both diffusion and exchange. This limitation was targeted by performing experiments where CO₂ was injected continuously into the spacer volume to maintain a high driving force. To evaluate the effect of diffusion length multi-fractured core samples were used, which demonstrated that length was not the dominating effect on core scale. An additional set of experiments is presented on non-fractured samples, where diffusion-limited transportation was assisted by continuous CO₂ injection and CH₄ displacement. Loss of permeability was addressed through binary gas (N₂/CO₂) injection, which regained injectivity and sustained CO₂-CH₄ exchange.

Keywords: CO₂ sequestration; CO₂ exchange; gas hydrate production; temperature effects; diffusion; exchange driving force

1. Introduction

Gas hydrates are a solid state of gas and water stabilized at high pressure and low temperature regimes. Vast energy resources are associated with gas hydrates, where different models suggest that hydrates contain 10^{15} to 10^{17} m³ CH₄ at standard temperature and pressure (STP) [1–3]. In comparison, the annual gas consumption in the US is about 7×10^{11} m³.

CH₄ provides advantages such as high enthalpy upon combustion and low carbon imprint. Focus is therefore shifted on sources of natural gas as the demand for cleaner energy continues to increase with global awareness of anthropogenic climate change. The immense energy locked in gas hydrates suggests that gas hydrates have the potential for becoming a major player in the future energy mix. Current challenges mostly relate to economics, as these resources are deposited in remote permafrost areas and often in challenging marine environments. The emergence of economically feasible gas production from hydrates may be within reach as technological advances and research effort continue to enhance the current hydrate knowledge base.

Depressurization is a favored approach to gas production from hydrates where minor energy is required to promote dissociation. The technology is already available from the conventional oil and gas industry, and the approach offers favorable terms in Class 1 reservoirs where the bottom of the hydrate bearing zone intersects the three-phase equilibrium line. Obvious limitations are endothermic decomposition, production of associated water and possible loss of geomechanical stability.

CH₄ production from gas hydrates may also be approached through guest replacement where the injected gas phase (e.g., CO₂ or N₂) provides a thermodynamically preferred gas hydrate [4] and replaces the CH₄ molecule within the hydrate cavity. This approach is based on minimization of Gibbs free energy. Figure 1 compares phase diagrams for different guest molecules, where CO₂ is thermodynamically preferred at certain temperature regimes. The exchange process is exothermic, where liberated heat during CO₂ hydrate formation [5] exceeds that required to dissociate CH₄ hydrate [6]. The exchange rate is therefore dependent upon the degree of subcooling, where Jung, *et al.* [7] suggested that liberated heat assists in the exchange process for subcooling up to 10 K. However, the contribution on exchange performance is sensitive to the fluids occupying the pores and the composite thermal conductivity of the hydrate-bearing sediments (HBS) which will impact heat transport from the reaction site. Another potential approach is injection of a binary gas mixture tailored to cause a positive synergy where permeability is maintained while CO₂-CH₄ exchange occurs in the hydrate crystal. N₂ is a less favorable hydrate former than CH₄ and CO₂, requiring higher pressure condition to form hydrate (see Figure 1), and may destabilize the existing CH₄/CO₂ hydrate at lower pressures. Adding N₂ to the injective mix therefore facilitates decomposition of CH₄ hydrate and minimizes CO₂ hydrate formation in excess brine. Gas hydrates have also been considered a potential environmental hazard, where uncontrolled dissociation could have severe consequences [8]. Permafrost thawing and temperature increase in HBS induces seeps of CH₄ through the crust. CH₄, although relatively short-lived in the

atmosphere (approximately 10 years), is a potent greenhouse gas that absorbs infrared radiation approximately 25 times more efficiently than CO₂ [9]. Enhanced hydrate stability can be accommodated through CO₂ exchange while benefitting from gas production and maintained structural integrity [10,11]. Other benefits are reduced seepage where CO₂ hydrate itself becomes an additional sealing layer [12].

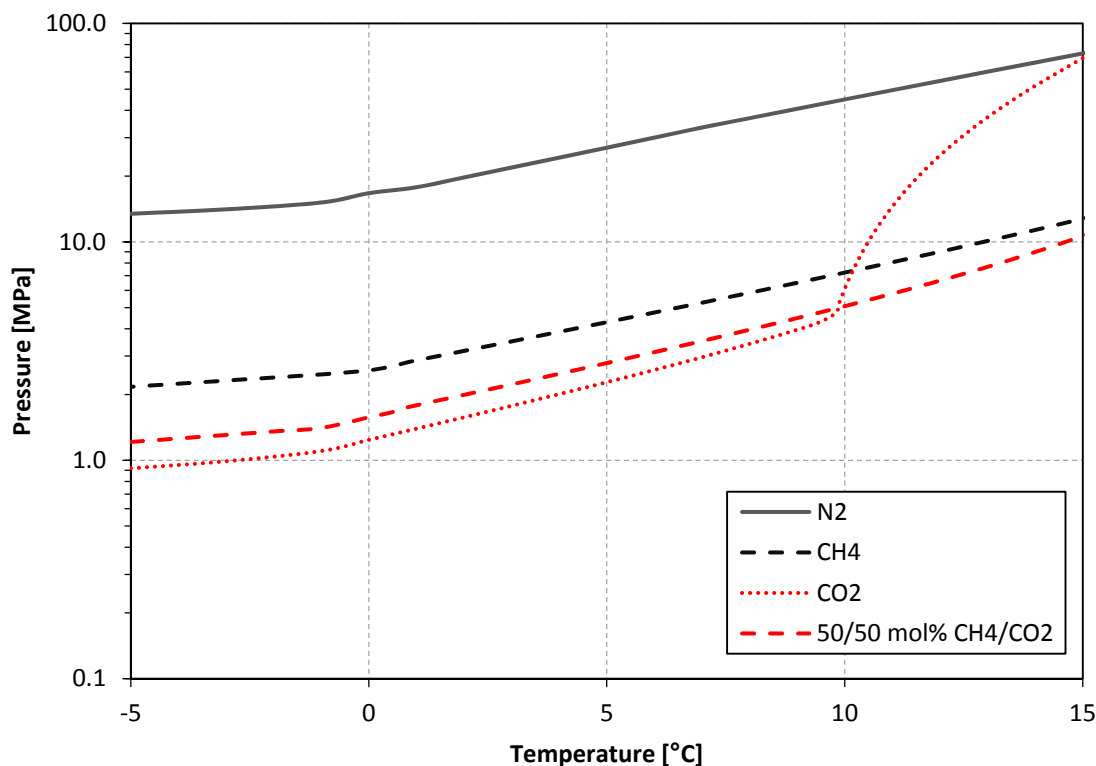


Figure 1. Comparison of stability for different guest molecule combinations. Pure CO₂-hydrate is thermodynamically more stable relative to pure CH₄-hydrate at certain temperature regimes, which is also observed for a binary gas composition of CH₄ and CO₂. The plotted equilibrium three phase line is based on gas composition, and does not necessarily reflect the hydrate composition. N₂ does not stabilize hydrate cavities at the experimental conditions, but is included for comparison. Data generated using CSMGem [13].

The exchange technology has previously been demonstrated in bulk experiments [14–17], in sediments [18–24] and numerically [19,25,26]. This work is part of the laboratory work that was conducted in advance of the Ignik Sikumi field test [27], where the University of Bergen in partnership with ConocoPhillips have studied CO₂-CH₄ exchange for a range of initial saturations. A single well was drilled in April 2011, intersecting multiple potential hydrate intervals at Ignik Sikumi [27]. In 2012, 2609 kg CO₂ and 5479 kg N₂ (77/23 mol% N₂/CO₂) was injected into the Sagavanirktok “Upper C” sand with S_h averaging at 75% and a thickness of 30 ft. Compositional analyzes of gas produced during flow-back revealed 22 mscf CO₂, 155 mscf N₂ and 821 mscf CH₄. The test has so far been considered a success [28].

Lee *et al.* [14,15] reported that 64% of the CH₄ in hydrate (powdered solid hydrate) were replaced by CO₂. The exchange process occurred fast, but they indicated that the sample morphology could play an important role for the conversion efficiency (potentially higher conversion with finer grinding). Initial CO₂-CH₄ exchange at the surface of a hydrate volume will result in a layer of CO₂ hydrate that isolates the original CH₄ hydrate volume. Continued conversion requires that the CH₄ hydrate is exposed to CO₂, and mass transfer will therefore be a limiting factor in such a scenario. Variation in hydrate morphology (e.g., protrusions of dendrites or lobes into the water) may on the other hand contribute to increased reaction surfaces and therefore benefit the exchange performance.

Water will usually be the wetting phase when water and gas are present in a porous media. Capillary bound water will typically remain at the mineral surfaces after gas hydrates have formed as the hydrate is unable to attach to the mineral surfaces due to incompatibility between the surface hydrogen bonded water molecules and geometrical structures of partial charges on atoms in surfaces of minerals. A water film of varying thickness will therefore separate the mineral and hydrate surface, in which gases (CH₄ and/or CO₂) may be transported. The diffusion coefficient of CO₂ and CH₄ in water [29] are several orders of magnitude larger than diffusion through hydrate [30,31]. Mass transfer will therefore be more efficient in the water layer, which is important for the exchange mechanism [19], as limited mass transport through solid hydrate layers will impair the exchange performance. This study will evaluate the performance of the exchange technology through comparison of multiple experiments with varying flow conditions and driving force.

2. Experimental Description

2.1. Experimental Design

The first experimental setup took advantage of a superconducting Unity/Inova-Imaging 85/310 spectrometer MRI from Varian Inc. (Palo Alto, CA, USA) which operated at a resonance frequency of 87.5 MHz (corresponding to approximately 2 Tesla magnet). The MRI provided continuous spatially resolved saturation data during operation. Hydrogen in hydrate has a short relaxation time, and is not visible with standard spin-echo techniques. Loss of signal therefore indicates hydrate formation. Full 3D images were acquired every 2 h and 17 min, while 1D saturation profiles could be collected in a few seconds. One of the advantages of the MRI is that the signal intensity is proportional to hydrogen density, and it can therefore be used to substantiate presence of water and CH₄ through comparison with MRI intensity at known saturation. The water signal is more substantial than CH₄ due to higher hydrogen density and water will therefore dominate the measured signal in the pore space. Capillary bound water has less contribution, while signal from CH₄ in pore space is close to the measured background signal at the settings used in this study. Two accurate Quizix C-6000-10HK-HC-HT high pressure pumps from Chandler Engineering (Tulsa, OK, USA) were used for pore pressure control (CH₄, CO₂, N₂ or binary gas mixtures), as illustrated in Figure 2. Digiquartz pressure transducers by Paroscientific Inc. (Redmond, WA, USA) measured inlet and outlet line pressure, while an additional sensitive transducer monitored differential pressure. A Quizix QX-6000 pump pressurized and circulated Fluorinert FC-40 (3MTM, Minneapolis, MN, USA) for overburden and temperature control. The Fluorinert is compatible with the MRI due to its dielectric properties and absence of hydrogen.

Temperature was monitored by a type-T thermocouple positioned within the confining fluid, which was maintained constant at 4.0 ± 0.3 °C during operation. Additional description of the experimental setup may be found elsewhere [32,33].

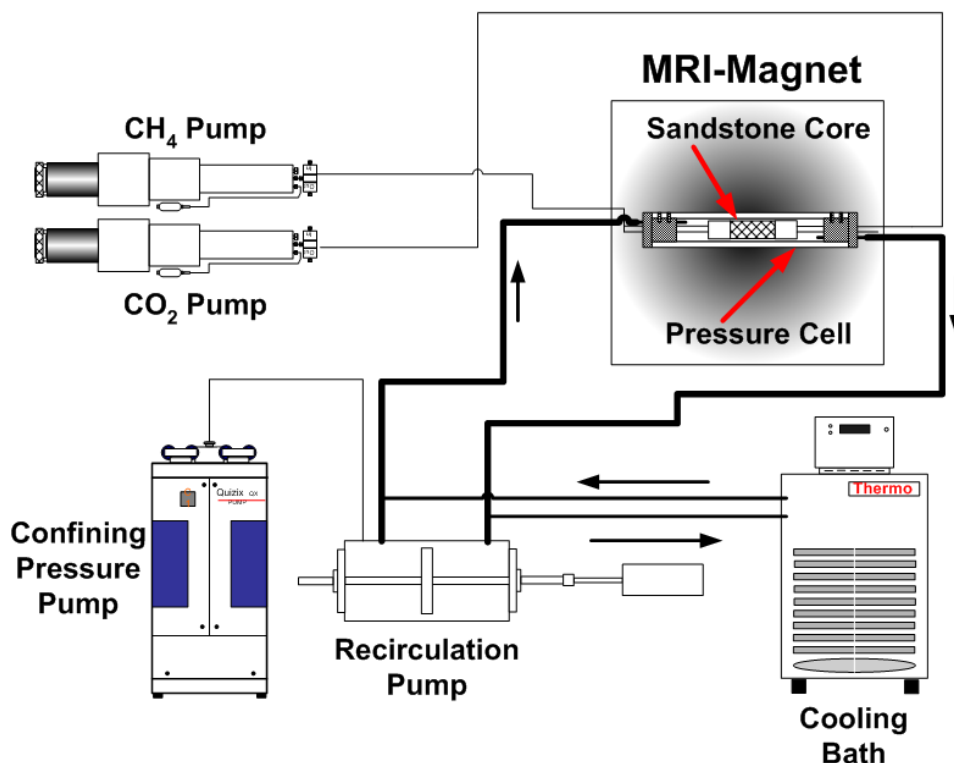


Figure 2. Illustration of the experimental setup applied for the majority of this study. The setup is equipped with a 2 Tesla superconducting MRI, which gives the advantage of *in situ* spatially resolved saturation data. The system is equipped with two high precision pumps for pore pressure, and a complex high pressure system for cooling and overburden pressure.

Accurate high pressure pumps (either Quizix C-5000-2.5K-HC or Sanchez Technology (Viarmes, France) Stigma 300) were used for pore pressure (gas or water) in the second experimental setup (see Figure 3). Custom designed Druck UNIK 5000 pressure sensors (General Electric, NY, USA) were monitoring differential, inlet and outlet pressure with a 0.04% FS sensitivity. Overburden pressure was provided by air-driven Haskel (Burbank, CA, USA) MS-71/MS-188 liquid pumps (mineral oil) in combination with gas-loaded accumulators for improved pressure control.

The setup was equipped with an in-line Agilent (Santa Clara, CA, USA) 3000A gas chromatograph (GC) that measured gas composition at specified intervals. CH₄ production was quantified in real time by using a Bronkhorst (Ruurlo, The Netherlands) M13 Coriolis mass flow meter (MFM) in combination with the GC. The GC inlet pressure was reduced through a combination of a gas-loaded Hastelloy Equilibar (Fletcher, NC, USA) EB1ZF1 Zero Flow Precision back pressure regulator and a spring-loaded Swagelok (Solon, OH, USA) KLF High-Sensitivity back pressure regulator. Cooled antifreeze was circulated in cylindrical cooling jackets that confined the core holder, and was maintained at 4.0 ± 0.3 °C during operation.

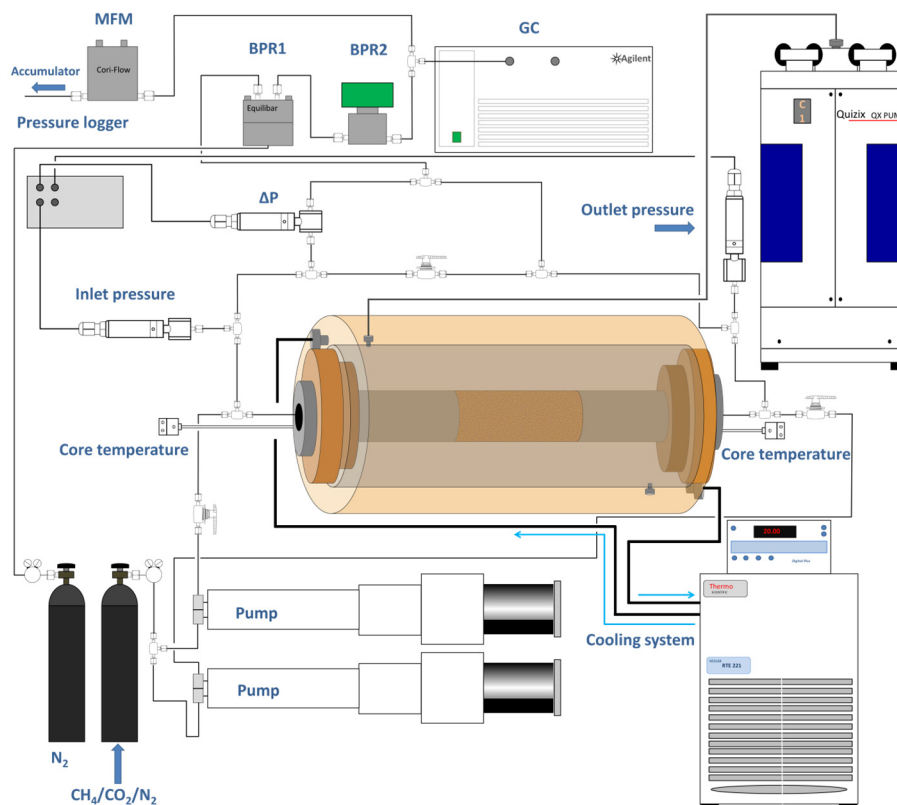


Figure 3. Illustration of the second experimental setup, where an *in line* GC and mass flow meter assisted in determining the effluent gas composition.

Bentheim sandstone was used for all experiments in this study because of its uniform properties (average pore diameter: 125 microns, porosity: 0.23–0.25, permeability: 1.1 D). The core dimensions ranged from 9.96–14.55 cm in length and 3.74–5.06 cm diameter (see Table 1). Three different core configurations were used, as illustrated in Figure 4. The longitudinal fracture was maintained open by a polyoxymethylene (POM) spacer that provided increased surface area for CO₂ exposure and a known accumulation volume where CH₄ production was monitored *in situ* by MRI.

Table 1. Summary of core dimensions, initial saturation and temperature during exchange for samples used in this study.

Paper name	NaCl concentration (wt%)	Swi (Frac)	Core length (cm)	Core diam. (cm)	Porosity (Frac)	Temp. (°C)
SS1	0.1	0.45	9.96	3.81	0.24	4.0
DS1	3.0	0.50	10.08	3.81	0.24	4.0
DS2	0.1	0.50	10.08	3.81	0.24	4.0
c1 to c6	0.1	0.3–0.6	10.00	3.74	0.24	4.0
w1	3.5	0.51	10.01	3.74	0.24	4.0
w2	0.1	0.41	14.55	5.06	0.25	4.0
w3	0.1	0.41	14.52	5.06	0.24	4.0
w4	0.1	0.43	14.14	5.06	0.24	9.6
w5	3.5	0.67	14.54	5.06	0.24	4.0
w6	3.5	0.64	13.67	5.05	0.23	4.0



Figure 4. Three different core configurations were applied in this study. The fractured design was applied to maximize and provide constant reaction interface while maintaining flow conditions. A double-spacer design was applied to address limitations in diffusion length, while the non-fractured sample was used for more realistic scenarios.

2.2. Experimental Procedure

Each sample was partially saturated with a predetermined brine solution. Saturations ranged between 0.3 and 0.6 with salinities between 0.1 wt% and 3.5 wt% NaCl (see Table 1). The samples were positioned within high pressure vessels where pore- and overburden pressure was increased incrementally to 8.38 MPa and 10.44 MPa, respectively. The system temperature was reduced by circulating cooled anti-freeze and typically maintained at 4.0 ± 0.3 °C during operation. Hydrate formation was detected as a drop in MRI intensity and decrease in pump volume, as the gas phase becomes more concentrated in the highly organized hydrate crystal. Good agreement between mass balance data and MRI was generally observed, as illustrated in Figure 5. The system was assumed to be at equilibrium when only minor changes were observed in CH₄ consumption and MRI intensity.

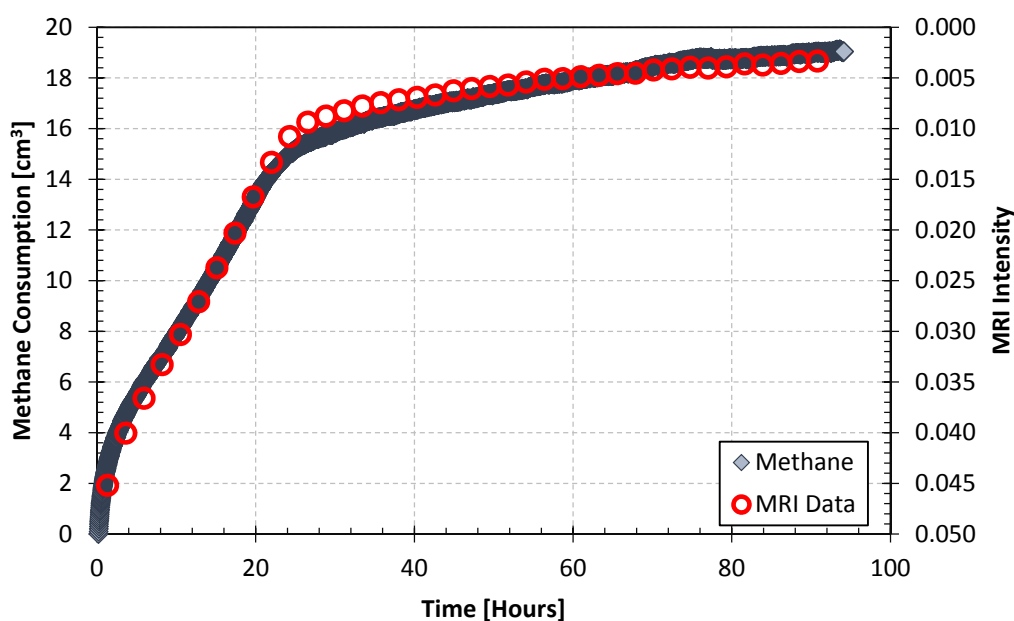


Figure 5. Comparison of CH₄ consumption and MRI intensity during hydrate formation for experiment c4 ($S_{wi} = 0.6$). MRI intensity is plotted using inverse scale for easier comparison.

Hydrate saturation was quantified based on CH₄ consumption from the pump and the MRI intensity. While saturation based on MRI is inversely proportional to intensity, the mass of water converted to hydrate based on pump logs was calculated by the following equation:

$$m_H = \nu \cdot \left(V_{CH_4} [\text{cm}^3] \cdot MD_{CH_4, 23^\circ\text{C}} \left[\frac{\text{mol}}{\text{cm}^3} \right] + V_{exp} [\text{cm}^3] \cdot MD_{CH_4, 4^\circ\text{C}} \left[\frac{\text{mol}}{\text{cm}^3} \right] \right) \cdot M_{H_2O} \left[\frac{\text{g}}{\text{mol}} \right] \quad (1)$$

where m_H is the mass of hydrate formed from water; ν is the hydration number, 5.99 (based on observations from [34]); V_{CH_4} is the volume of CH₄ injected from the pump in order to maintain constant pressure during formation; MD_{CH_4} is molar density of CH₄ at 23 °C and 4 °C for calculation related to pump volume and pore volume respectively; V_{exp} is the expansion component as given by Equation (2) and M_{H_2O} is the molar mass of water. A correction factor was implemented due to water expansion (26%) during hydrate formation:

$$V_{exp} = \frac{m_H [\text{g}]}{\rho_{H_2O} \left[\frac{\text{g}}{\text{cm}^3} \right]} \cdot 26\% \quad (2)$$

where ρ_{H_2O} is the density of water. It can be noted that Equations (1) and (2) are not independent and must be solved simultaneously. Iteration was therefore used to calculate the saturation. Given a density of water ρ_{H_2O} and the respective pore volume V_{pore} , hydrate saturation was then calculated as:

$$S_H = \frac{m_H / \rho_{H_2O} \cdot 1.26}{V_{pore}} \quad (3)$$

CO₂ injection and exchange occurred either through huff-and-puff or continuous constant rate injection. For the first approach, CO₂ was injected into the spacer volume to displace excess CH₄, which was confirmed through 11 sagittal MRI profiles. The outlet valve was closed after the flush, while inlet maintained constant CO₂ pressure. MRI 3D images were used to monitor intensity changes during the CO₂ soaking period, which lasted up to 600 h for each flush. The CO₂ was replenished when only minor intensity changes were observed.

CO₂ was injected continuously at 0.033 cm³/min either through a fractured or whole sample to address driving force issues for both mass transfer and exchange kinetics. The injection occurred over several days, and the gas composition was determined by an in line GC. Flow issues and plugging were observed for some samples (non-fractured samples), which were either approached through constant ΔP injection or injection of a binary gas mixture (N₂ and CO₂). The produced CH₄ (n (mol)) was found by multiplying the fraction of CH₄ with cumulative moles produced, as described in Equation (4):

$$n_{CH_4} = \sum_{j=0}^n \frac{m_j \cdot X_{CH_4,j}}{M_j} \quad (4)$$

where m_j is the mass produced of all fluids; $X_{CH_4,j}$ is the CH₄ fraction; and M_j is the average molar mass during time step j . The recovery was further quantified by dividing the cumulative produced CH₄ corrected for line volume by the total number of moles in the system.

The inherent hydration pressure varies as a function of guest composition, and the dissociation pressure can therefore be used to estimate the conversion efficiency. This method assumes equilibrium

between the gas occupying the pore space and the gas within the hydrate cavities. The depressurization sequence was initiated by pressure drawdown above the equilibrium line for pure CH₄ hydrate. Reformation from excess CO₂ during decomposition was minimized through CH₄ injection until only traces of CO₂ were observed in the effluent. Further depressurization occurred in 0.07–0.21 MPa steps while monitoring both pump volume data and MRI. Each pressure reduction step involved a ramp down period, where the pump was programmed to perform the pressure reduction step over a 20 min period. Constant pressure was then maintained for 4.2 h while acquiring two MRI images at each pressure step before the following ramp-down period was initiated. Hydrate compositions were then determined by comparing dissociation pressures with statistical equilibrium data from CSMGem [13], where extent of dissociation was reflected by variations in MRI intensity (MRI intensity = 1 indicates no hydrate, while MRI intensity = 0 indicates all hydrate).

3. Experimental Results and Discussion

3.1. Diffusion Driven Mass Transport—a Short Review of Previous Experimental Efforts

Single spacer configurations have been emphasized in previous experimental effort by the University of Bergen, where diffusion-driven mass transport formed the basis for investigating the CO₂-CH₄ exchange process. CO₂ diffusion into core segments resulted in accumulation of CH₄ into the spacer volume as CO₂ reacted with CH₄ hydrate. The efficiency of diffusion driven CO₂ transport and the exchange driving force are both functions of the CO₂ concentration in the gas/liquid phase and therefore sensitive to dilution during exchange. Contamination by released CH₄ reduced the efficiency of the injected CO₂, but estimates suggested that approximately 50%–85% of the CH₄ originally converted into CH₄ hydrates was recovered through CH₄-CO₂ exchange based on a “huff-and-puff” approach [32]. MRI intensity variations for both core halves and the spacer volume for sample SS1 are compared in Figure 6. By revisiting one of the diffusion experiments we can make several useful observations;

1. Immediate production response was observed in the spacer volume after pure CO₂ was injected into the spacer volume (injection occurred after 48 h and 670 h and lasted for 5 min before the system was shut in and the CH₄ hydrate was soaked in the injected CO₂). The production response is reflected by increasing MRI intensity (grey triangle) which indicates increased CH₄ concentration in the spacer volume.
2. Immediate intensity drops were observed in both core halves after CO₂ was flushed through the spacer volume. Initial CO₂ transportation is therefore not necessarily a slow process, but decreasing CO₂ gas/liquid concentration during exchange may prevent mass transfer to radially more distant core segments. This will eventually affect the recovery unless CO₂ is replenished. The majority of the injected CO₂ will be channeled through the low resistance conduit (the spacer volume) during the 5 min flush. The advection-driven CO₂ mass transport within the low-permeable CH₄-hydrate saturated sediment was therefore not assumed to be significant, although some CO₂-CH₄ displacement was anticipated, especially at the core surfaces facing the open spacer volume. The fluid flow regime was strictly diffusion-driven after the shut-in.

3. The monotonically increasing intensity trend in the core halves indicates exchange and release of CH₄ with subsequent reduced exchange driving force. This is reflected in the spacer intensity curve shape, where the derivative of the curve trajectory approaches 0.

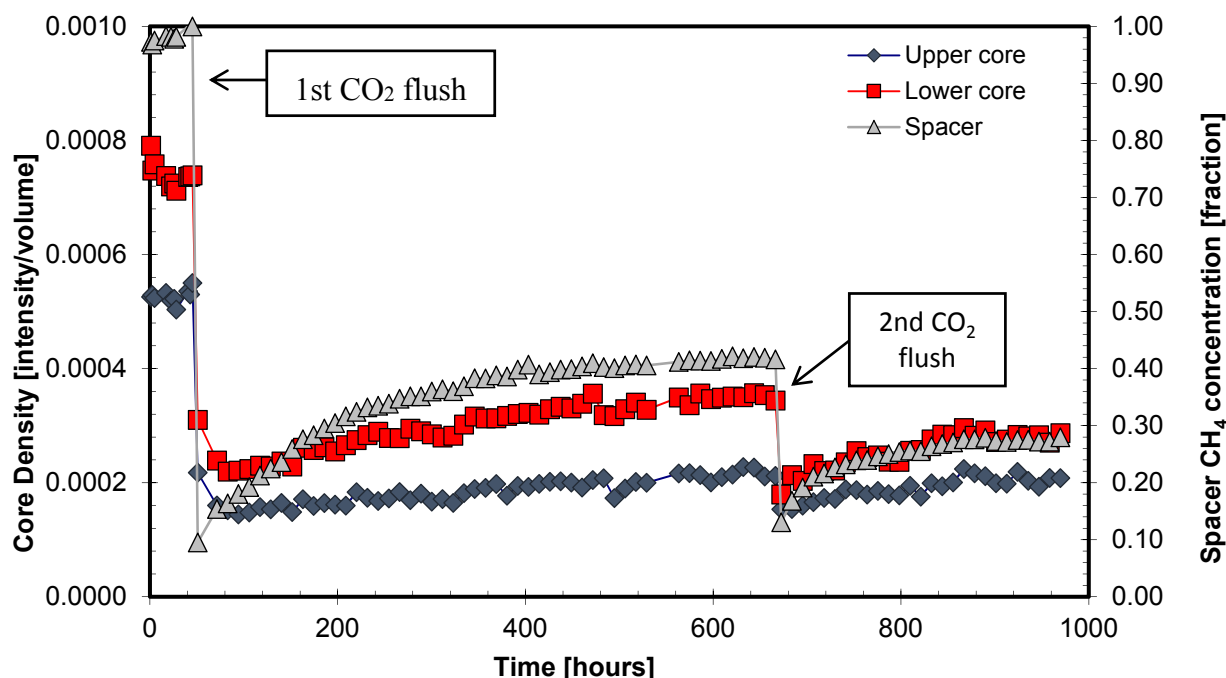


Figure 6. Comparison of intensity progression in the two core halves and spacer volume during CO₂ injection and exchange. The hydrogen density is efficiently reduced as CO₂ diffuses into the core segments. The slight monotonically increasing trend suggests release of CH₄ as a result of exchange. Each image was acquired over 2 h and 17 min.

3.2. Salt Effects during Exchange

Possible exchange limitations imposed by the diffusion length were addressed through two experiments utilizing the double spacer configuration. The reaction interface between the open spacer volume and core was efficiently increased by adding a second fracture, while the diffusion distance was minimized. No significant differences were observed in production in Figure 7 relative to anticipated trends from the single spacer experiment (see comparison in Figure S1), and other mechanisms such as ion concentration appeared to be dominating the exchange performance. Intensity variations within the core segments indicate CO₂ hydrate formation and/or CO₂-CH₄ exchange as CO₂ was introduced to the sample (see Figure S2). A series of hydrate formation experiments with varying salinity demonstrated how the fraction of crystallized water was reduced for higher salinities because of increased ion interaction with the formation water [33]. Differences in residual water after hydrate formation was also observed in this study ($X_{\text{NaCl}} = 3 \text{ wt\%}$: $S_w = 0.081$, $X_{\text{NaCl}} = 0.1 \text{ wt\%}$: $S_w = 0.023$ (see Figure S2)). Salt ions are excluded from the crystallized hydrate structure during hydrate formation, and the relative ion concentration in the remaining formation water therefore increases as gas hydrates form. The fluid distribution within the sediment is controlled by surface chemistry and intrinsic physical sediment properties, which typically causes the water to reside along the quartz

minerals and in the smaller pores, while gas is distributed within the pore space preferably in the larger pores. Persistence of a non-frozen layer along the grain surface could facilitate the exchange performance by acting as distribution channels for the injected CO₂ [19]. The impact of these channels would be more significant in a high-salinity scenario, where additional water remains un-frozen and contributes as transportation channels. In analogy, 10%–40% ion retention in microscopic layers between ice structures was observed for sea ice growth (high salinity) while lake ice (low salinity) growth progressed in a planar manner [35]. Presence of water layers between poly-crystal hydrate would have a significant impact on the surface reaction area and subsequently the mass transfer. Still, we need to keep in mind that there are other effects that come into play which may impact the observed trends. Higher NaCl concentration will have a thermodynamic impact on the hydrate stability. CH₄ hydrate formation (at the experimental conditions) is inhibited at 14.9 wt% NaCl concentration, while CO₂ hydrate formation is more susceptible to ion interaction and is retained at approximately 10.6 wt% NaCl brine concentration, as demonstrated in Figure 8. Abundance of NaCl will also result in less favorable conditions in terms of solubility [36]. Elevated salinity appears to impact the CO₂-CH₄ exchange in this study; however, we cannot conclude if this effect only relates to improved mass transfer due to water availability or if there are additional effects of the salt that impact the exchange efficiency.

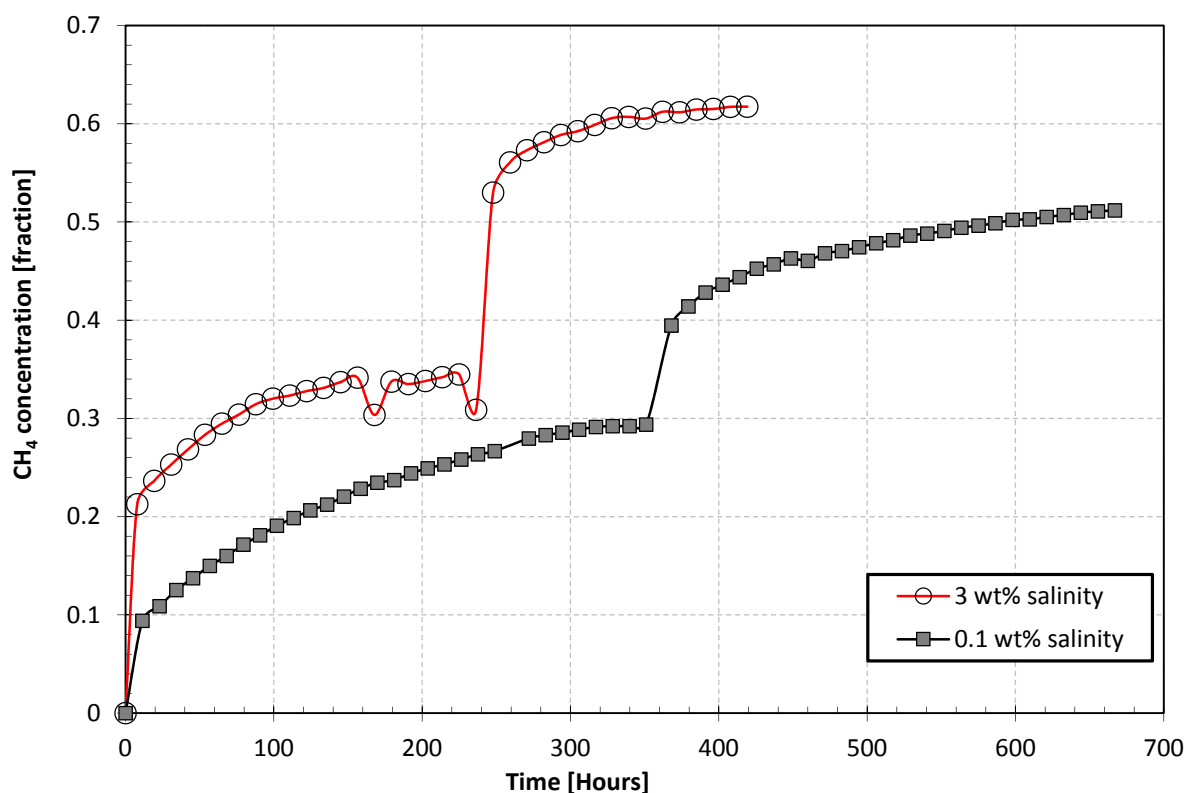


Figure 7. CH₄ accumulation in the spacer volume was more significant for the higher salinity experiment (red line, open black circles), which suggests that there may be an effect of elevated salinity on the CH₄ release.

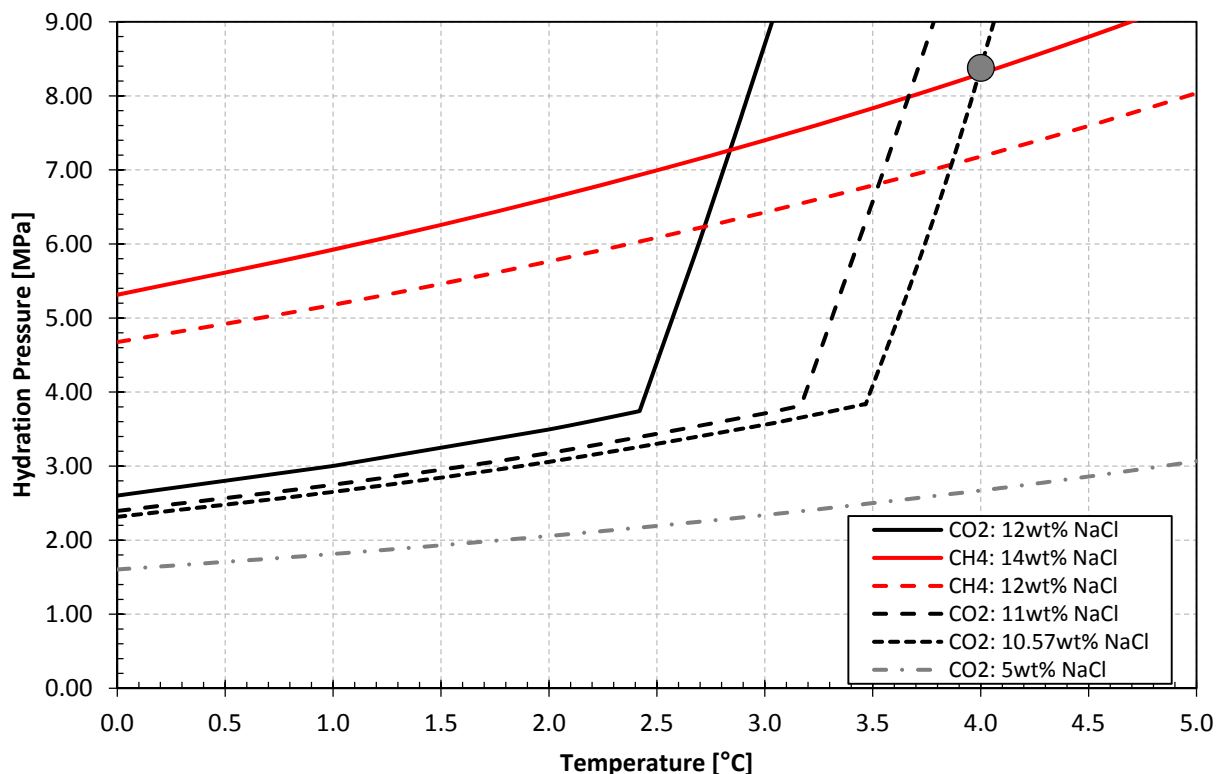


Figure 8. Hydrate three-phase equilibrium lines at varying salinities for CH₄ and CO₂ guest molecules. CH₄, represented by the red lines, is less susceptible to variations in ion concentration than CO₂. Gas hydrate formation at the experimental conditions (marked by the grey circle) will be inhibited at 14.9 wt% NaCl for CH₄ hydrates and 10.6 wt% NaCl for CO₂ hydrates.

3.3. Maximizing Conversion Efficiency through Continuous CO₂ Flow

Limitations in mass transport and exchange efficiency were addressed through a series of experiments where CO₂ was continuously injected through the spacer volume. Advection-driven transportation offers two important mechanisms: (1) high CO₂ concentration with subsequent high exchange driving force; and (2) continuous transportation of released CH₄. The non-tortuous fracture design will serve as a high flux conduit where most of the CO₂ is channeled through. The transport mechanism was therefore diffusion-dominated, but the transport efficiency was maximized by maintaining high concentration CO₂ in the system.

Six single spacer experiments (c1-c6) were conducted on a single sample for months of operation, where hydrates were formed, exposed to CO₂ and depressurized to estimate final hydrate composition [21]. Two different initial water saturations ($S_{wi} = 0.3$, $S_{wi} = 0.6$) were used, where differences in spatial saturation distribution varied (the water distributions for c1 ($S_{wi} = 0.3$) and c4 ($S_{wi} = 0.6$) were heterogeneous, while the other experiments were characterized by fairly homogeneous saturation conditions; see Figures S5 and S6, for saturation distribution of c4 and c5; c1 ($S_{wi} = 0.3$) and c4 ($S_{wi} = 0.6$) were heterogeneous, while the other experiments were characterized by fairly homogeneous saturation conditions). c1 was designed identical to previous single spacer experiments, where mass transportation

was strictly diffusion driven, and therefore served as a reference experiment. The additional five experiments were performed with slight variations in saturation and exposure time (CO₂ soaking), where each cycle included;

1. Hydrate formation at 4 °C and 8.38 MPa.
2. Injection of CO₂ at 10 cm³/min to displace excess CH₄ in the spacer volume after hydrate formation. MRI profiles (sagittal images of the spacer volume) were acquired during injection to confirm displacement.
3. CO₂ was injected at 0.033 cm³/min for several days (2–5) during the exchange process itself.
4. Depressurization sequence to determine mixed hydrate composition.

As previously mentioned, the dissociation pressure varies as a function of guest composition. Correlating dissociation pressure to guest composition was achieved through CSMGem [13], while MRI changes were used to determine the extent of dissociation during the controlled depressurization sequence. Figure 9 summarizes the depressurization sequence for all six single spacer experiments (c1–c6), where one additional whole core experiment has been added for comparison (w1). Normalized MRI intensity is displayed on the y-axis, while mol% CO₂ in hydrate and pressure is displayed on the x-axis. Increasing MRI intensity between two data points indicates dissociation, where the extent of dissociation is reflected by the change in MRI intensity (MRI intensity = 1 means no hydrate). A steep curve in Figure 9 represents fairly homogeneous conversion (see c3), while a gradual curve indicates a range of conversions (and therefore a non-uniform final hydrate composition), as seen for the whole core sample (w1).

The first cycle (c1) was designed as a reference experiment, and therefore utilized the huff and puff procedure, while exchange in remaining cycles (c2–c6) was maximized through constant CO₂ injection through the spacer volume. In Figure 9, a small decrease in MRI intensity (the hydrogen density decreases slightly, especially in the gas phase, as the pressure is reduced) is observed for c1 (blue square) as the pressure was reduced from 4 to 3 MPa. The MRI intensity increased from 0.11 to 1 in the following step, thus indicating that 40%–58% CH₄ was replaced by CO₂ after 9 days of soaking in the huff and puff approach. In comparison, 2 days of constant injection (c2–purple diamonds) at 0.033 cm³/min induced 58%–65% recovery. The exchange was further enhanced by 10% through c3 (green circles), where the injection/soaking period was extended by one day. To summarize, the dissociation pressure was reduced during constant injection with continuous replenishment of CO₂, as illustrated in Figure 9. The fraction of CO₂ within hydrate was higher during continuous injection, relative to the huff and puff approach, even for a shorter soaking time. The exchange rate in the huff and puff procedure is limited by CO₂ dilution from CH₄ influx in the spacer volume, reducing the exchange efficiency, while continuous replacement in the CO₂ enhances the diffusion rate of CO₂ into the core halves. The results are also summarized in Table 2.

Table 2. Summary of experimental conditions and results for data illustrated in Figure 9.

Test	Saturation	Exposure time (days)	Conversion	Comment
c1	0.3	9	40%–60%	Huff and Puff. Non-uniform saturation distribution. Mass transport based on diffusion.
c2	0.3	2	58%–65%	Constant CO ₂ flow at 0.033 cm ³ /min. Uniform saturation.
c3	0.3	3	71%–78%	Constant CO ₂ flow at 0.033 cm ³ /min. Uniform saturation.
c4	0.6	3	14%–52%	Constant CO ₂ flow at 0.033 cm ³ /min. Non-uniform saturation, S _w exceeding 0.8 in some areas.
c5	0.6	5	71%–83%	Constant CO ₂ flow at 0.033 cm ³ /min. Uniform saturation.
c6	0.6	3	65%–71%	Constant CO ₂ flow at 0.033 cm ³ /min. Uniform saturation.
w1	0.5	3	16%–85%	Whole core. Constant CO ₂ flow at 0.033 cm ³ /min. Non-uniform saturation, plugging, significant residual water.

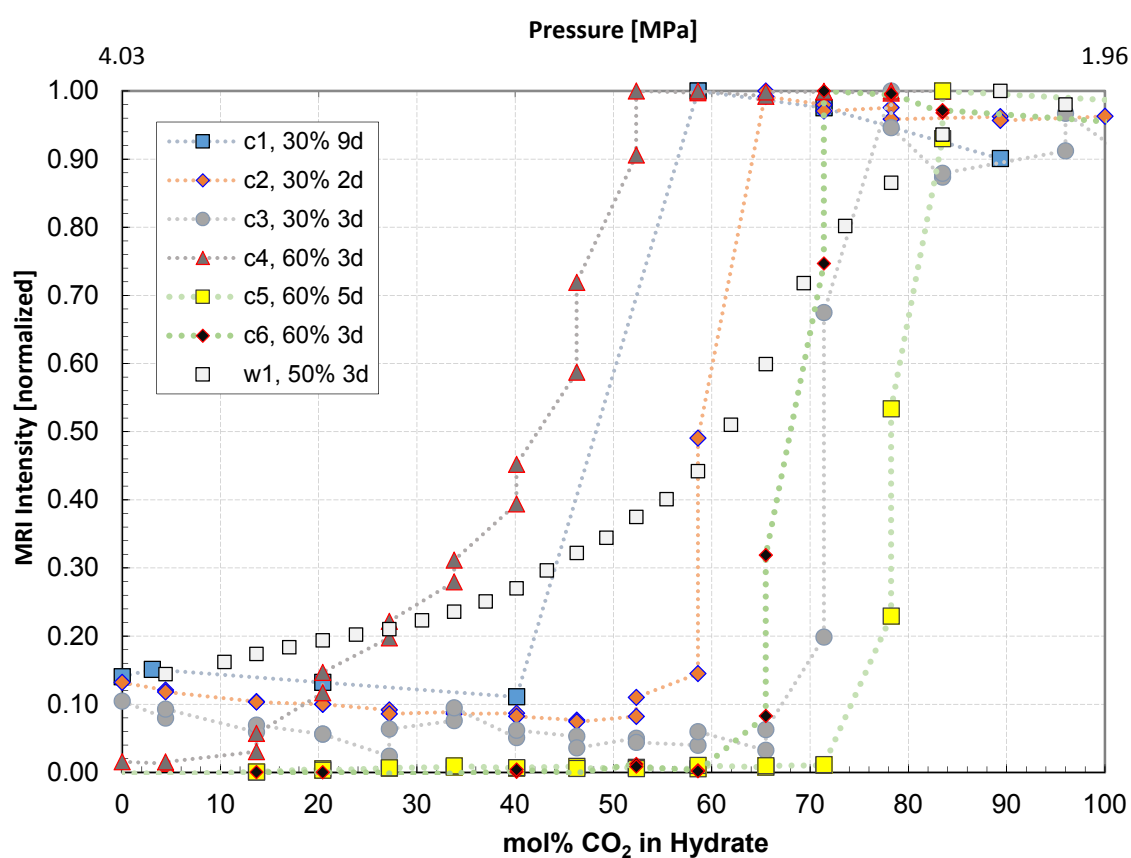


Figure 9. Comparison of overall exchange efficiency for different approaches during CO₂ exchange (c: cycle, w: whole core, *i.e.*, c1 is cycle 1, S_w = 0.3, 9 days exposure time). The method takes advantage of shifting hydration pressure with varying guest composition. The results demonstrate the importance of soaking the CH₄ hydrate in CO₂ for higher recovery, and indicate that mass transfer is a limiting mechanism in exchange kinetics.

Multiple pressure steps were required for complete dissociation for experiments c4 and w1, thus indicating fairly heterogeneous mixed hydrate composition. Non-uniform initial water saturation distribution with values exceeding 0.9 was observed for c4 (see Figure S4, for saturation histogram and Figure S5, for visualization of initial water saturation before hydrate formation). While presence of

excess water may be beneficial for the exchange process (relative to presence of solid hydrate), areas with high water saturation may adversely impact the subsequent exchange process if all the water is crystallized. Extended soaking times are necessitated by increase in hydrate volume due to the diffusive properties of CO₂ through hydrate. Initial reactions will occur at the surface of the CH₄ hydrate volume. The efficiency of the exchange process will therefore be impacted by a layer of CO₂ hydrate that confines the CH₄ hydrate. Changes in $V_{\text{hydrate}}/A_{\text{interface}}$ is described as $r/3$ for a spherically configured hydrate volume. Higher radius (increasing hydrate volume) will therefore yield unfavorable conditions from a mass transfer perspective.

Initial dissociation in c4 was focused in areas adjacent to the open spacer volume where exchange efficiency was limited by high S_{h,CH_4} , as illustrated in Figure 10. These areas were initially characterized by high water saturation (see Figure S5), which may indicate that these areas remained unexposed to CO₂ during the soaking period. In comparison, higher pressure drawdown (almost 1 MPa lower) was required to dissociate the mixed gas hydrate when the sample was initially uniformly saturated with water (Figure 11). This suggests that the conversion efficiency was better compared to the non-uniformly saturated sample. The exchange process was mainly rate-limited by mass transport, where 30%–40% recovery difference was observed between the uniformly (c6) and non-uniformly saturated sample (c4) at $S_{wi} = 0.6$. Non-uniform saturation conditions are unfavorable from an exchange perspective as local permeability reduction in regions with high hydrate saturation may decrease sweep efficiency while extended soaking times are required due to low diffusivity through bulk hydrate.

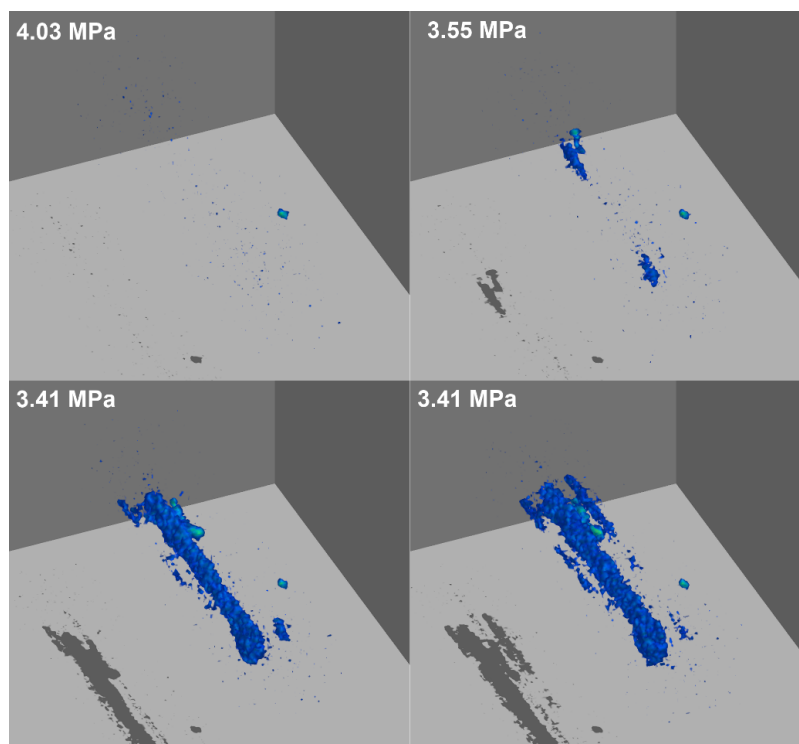


Figure 10. Cont.

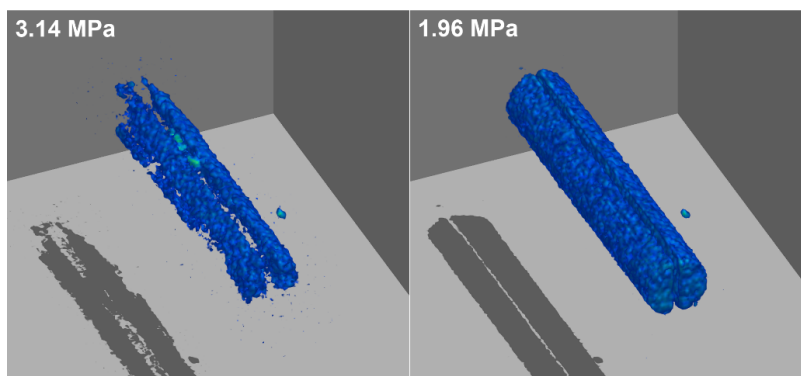


Figure 10. Depressurization sequence for sample c4. The initial water distribution was relatively heterogeneous, which resulted in areas with higher S_{h,CH_4} . These areas require longer soaking time, as diffusion through hydrate layers is a slow process. Six pressure steps were required for full decomposition of the multi-compositional hydrate.

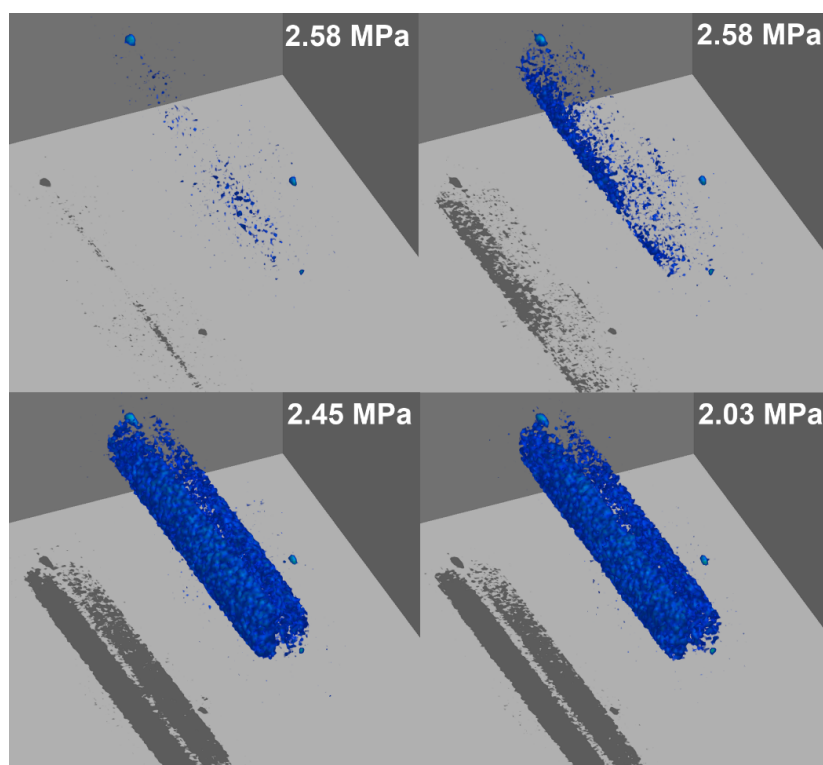


Figure 11. Decomposition of cycle c2 occurred mainly at 2.58 and 2.45 MPa, thus indicating a conversion of approximately 60 mol% CO_2 .

3.4. Continuous CO_2 Mass Transport in Non-Fractured Samples

A series of experiments were performed to facilitate transportation of CO_2 by constant injection through non-fractured samples. The experiments with a spacer demonstrated that longer soaking time yielded higher recovery. Reduced exchange efficiency due to CO_2 dilution was also documented during the huff and puff procedure. In theory, continuous CO_2 injection would offer favorable terms with enhanced transportation efficiency, where CO_2 is constantly replenished while released CH_4 is displaced towards the producer. To evaluate recovery as a function of injected CO_2 , the next

experiments were conducted with a mass flow meter, which in combination with the GC provided a measure of CH₄ produced during production.

CH₄ recovery curves for four non-fractured samples at different initial water saturation and temperature conditions are plotted in Figure 12 (see Table 1 for details). In contrast to pressure reduction procedures, this technique enables continuous evaluation of production in real time. The calculated recovery accounts for both free CH₄ gas in the pores and CH₄ as part of hydrate. Similar temperature and fluid saturation were observed in w2 and w3, and the reproducibility between the experiments was excellent. Both experiments indicate an ultimate recovery of approximately 50%, where 30% was recovered after injecting 1 PV CO₂.

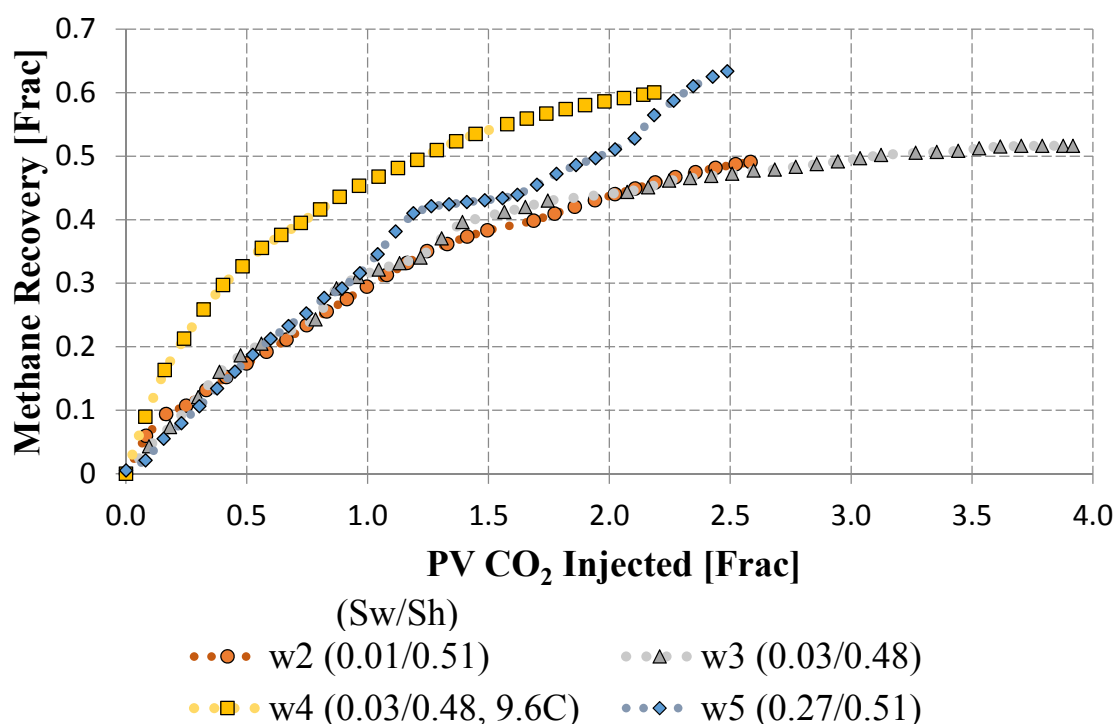


Figure 12. CH₄ recovery during constant CO₂ injection at 1.2 cm³/h over a 200 h period for four experiments. w2 and w3 have similar saturation and system temperature. w4 was performed at a higher temperature, while higher brine saturation was used for w5, resulting in residual brine saturation of 0.27. Co-injection of CO₂ and N₂ (25/75 mol%) was also necessary to maintain injectivity. The values in parenthesis represent residual water saturation and hydrate saturation.

Heat liberation during exchange is an important mechanism during CO₂ injection. The contribution is dependent upon the degree of subcooling ($\text{Subcooling} = T_{\text{equilibrium}} - T_{\text{sample}}$) and fluids occupying the pore space, where higher impact is anticipated for conditions in proximity to the CH₄ equilibrium line. w4 was conducted at higher temperature (9.6 °C), which shifted the degree of subcooling from 7.3 K to 1.7 K. The sample was therefore more susceptible to temperature changes associated with the exchange process, which was reflected in the higher replacement rate. 46% recovery was observed after injecting 1 PV CO₂, which is 53% higher than observations for samples at 4 °C. Liu *et al.* [24] studied exchange performance at various temperature and reported similar ultimate recovery although

the replacement rate was higher at elevated temperature. We have observed both higher exchange rate and final recovery (10%) in this study.

The Ignik Sikumi field trial in Alaska targeted the Eileen formation which is characterized by higher hydrate saturation (0.75) and a residual water saturation of 0.25 [37]. One of the experiments in this study was designed with higher water saturation ($S_w = 0.66$) to address challenges posed by the remaining excess water. The hydrate saturation after CH_4 consumption ceased was $S_H = 0.51$, and free water was also present ($S_w = 0.27$). A binary gas mixture (25/75 mol% CO_2/N_2) was used to avoid plugging the sample during injection. Co-injection of N_2 and CO_2 (77/23 mol%) was also used in the Ignik Sikumi trial, which continuously injected over a period of 14 days [38]. Similar effluent profile as the other experiments was observed for the first injected pore volume in w5, while a deviating trend was observed as injection continued. The effective gas permeability is significantly reduced when additional water is present, and the higher recovery may be linked to a change in the displacement front of the injected gas. The difference may also be a result of the gas composition itself.

3.5. Flow Remediation through Binary Gas Injection

Several experiments have been performed at the University of Bergen with a higher initial water saturation ($S_{wi} > 0.5$) which are characterized by the presence of free water after hydrate formation. Pure CO_2 injection resulted in drastically reduced permeability with little or no injectivity. Plugged samples were remediated through binary gas injection (75/25 mol% N_2/CO_2). N_2 does not preferentially stabilize guests at the experimental conditions, and the purpose is to maintain continuous flow while CO_2 may interact with the hydrate crystals. The extent of the interaction is dependent upon the local gas mixture at any point in time, as both excess and released CH_4 will impact the performance of the injected gas.

Effort to remediate a plugged sample is summarized in Figure 13. Inlet pressure was increased with pure N_2 at 237 and 261 h to remove hydrate films at the transaxial core faces and facilitate further fluid flow through the plugged sample. The CH_4 fraction remained high during binary gas injection, which indicates decomposition of CH_4 hydrate. The CO_2 effluent fraction was less than the injected fraction (black dashed straight line), which indicates that CO_2 replaced CH_4 in the hydrate cavities while N_2 prevented plugging. Positive synergy between optimized flow control and guest molecule replacement may therefore be achieved through binary gas injection. However, sonic measurements on samples have detected loss of stiffness during the replacement process [24,39]. This has also been supported by observed resistivity trends [33], which indicates rearrangement or decomposition of hydrates during binary gas injection.

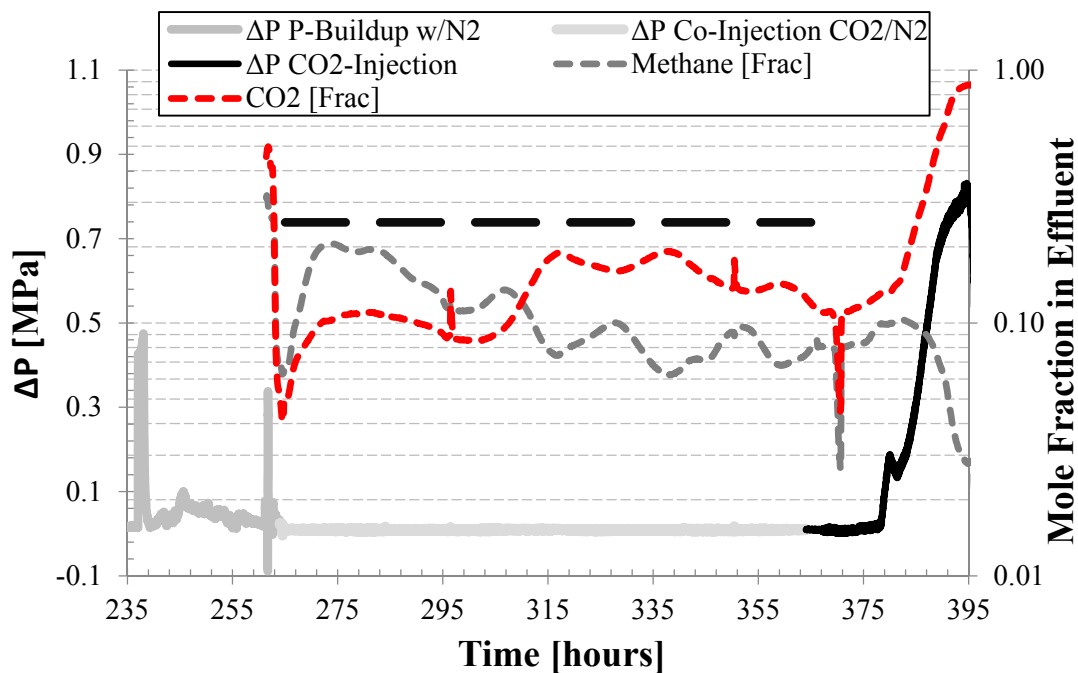


Figure 13. Effluent profiles suggest continued CO₂-CH₄ exchange during binary gas injection, as the CO₂ molar fraction was consistently less than the injected CO₂ fraction.

4. Conclusions

All experiments have demonstrated how CH₄-CO₂ exchange is a favorable approach where CH₄ gas production benefits from additional storage of CO₂. There was no apparent dissociation during this solid-liquid-solid transition, which suggests that the geomechanical stability was maintained. Replacement of CH₄ by CO₂ is therefore a promising approach for a sustainable energy future.

Mass transfer limitations from single spacer experiments were addressed through two double-spacer experiments where effective diffusion length was reduced. The experiments exhibited similar behavior, which may indicate that CO₂ concentration is more important than diffusion length for diffusion mass transfer at the experimental conditions. Single spacer experiments demonstrated how initial diffusion-driven mass transport is not necessarily a slow process, but the driving force for both mass transfer and exchange was reduced with decreasing CO₂ concentration.

CH₄ accumulation in the spacer volume was more significant for a high salinity experiment where the water content was more abundant at the initiation of CO₂ injection. Presence of liquid channels will improve the CO₂ mass transport relative to diffusion through hydrate; however, we cannot conclude if the observed trend is an effect of increased water content or by elevated salt concentration. Limitations in mass transfer and exchange driving force were addressed through a series of constant flow experiments, where conversion efficiency was related to soaking time and CO₂ concentration. Mass transfer and exchange driving force was maximized through constant injection, where final recoveries up to 85% were observed. 10% additional recovery was achieved by extending injection from 2 to 3 days. Lower hydrate saturation enhanced the exchange efficiency because excess gas provides favorable mass transfer conditions. The exchange process was confirmed through MRI and depressurization sequences where the binary hydration pressure was used for evaluation of final gas hydrate composition.

The majority of samples was uniformly saturated and displayed uniform final hydrate composition. Variations in saturation with subsequent higher local hydrate saturations resulted in reduced conversion, and multiple depressurization steps were required for dissociation of the hydrate indicating non-uniform conversion.

Constant CO₂ injection in non-fractured samples was favorable compared to the “huff-and-puff approach”, but was sensitive to heterogeneities and loss of permeability. Plugged samples were remediated by binary gas injection (N₂ and CO₂). This may have induced a positive synergy with good permeability and continued CO₂-CH₄ exchange.

Heat liberation associated with the exchange process appeared to have a significant effect on the recovery as conditions were shifted towards the three-phase equilibrium line of CH₄ hydrates. 46% CH₄ was recovered after injecting 1 PV CO₂, and the final recovery was 60%. Temperature susceptibility will be further addressed in future studies.

Supplementary Materials

Supplementary materials can be accessed at: <http://www.mdpi.com/1996-1073/8/5/4073/s1>.

Acknowledgments

Several experiments were performed in partnership with ConocoPhillips at the ConocoPhillips Technology Center (Bartlesville, OK, USA). The authors appreciate valuable contribution from Jim Stevens, James Howard and Keith Hester. We acknowledge the contribution from Christian Hågenvik, Reza Hossainpour, Truls Håheim and Hans Berge. Several of the authors are indebted to the Norwegian Research Council for funding.

Author Contributions

This work was a collaborative research effort between the four authors. The first author was the primary author of this article.

Nomenclature

S_i	Saturation of fluid i
n	Measure of fluid amount in moles
m	Measure of fluid weight
X_i	Fraction of fluid i
M_i	Molar weight of fluid i
MD_i	Molar Density of fluid i
ν	Hydration number
ΔP	Differential Pressure
PV	Pore Volume
V_i	Volume of fluid i
$A_{\text{interface}}$	Interface Area
r	Radius
T	Temperature

Conflicts of Interest

The authors declare no conflict of interest.

References

1. Kvenvolden, K.A. Methane hydrate—A major reservoir of carbon in the shallow geosphere? *Chem. Geol.* **1988**, *71*, 41–51.
2. Milkov, A.V. Global estimates of hydrate-bound gas in marine sediments: How much is really out there? *Earth-Sci. Rev.* **2004**, *66*, 183–197.
3. Klauda, J.B.; Sandler, S.I. Global distribution of methane hydrate in ocean sediment. *Energy Fuels* **2005**, *19*, 459–470.
4. Svandal, A.; Kuznetsova, T.; Kvamme, B. Thermodynamic properties and phase transitions in the H₂O/CO₂/CH₄ system. *Fluid Phase Equilib.* **2006**, *246*, 177–184.
5. Anderson, G.K. Enthalpy of dissociation and hydration number of carbon dioxide hydrate from the clapeyron equation. *J. Chem. Thermodyn.* **2003**, *35*, 1171–1183.
6. Anderson, G.K. Enthalpy of dissociation and hydration number of methane hydrate from the clapeyron equation. *J. Chem. Thermodyn.* **2004**, *36*, 1119–1127.
7. Jung, J.W.; Espinoza, D.N.; Santamarina, J.C. Properties and phenomena relevant to CH₄-CO₂ replacement in hydrate-bearing sediments. *J. Geophys. Res.: Solid Earth* **2010**, *115*, B10102.
8. Kennett, J.P.; Cannariato, K.G.; Hendy, I.L.; Behl, R.J. *Methane Hydrates in Quaternary Climate Change: The Clathrate Gun Hypothesis*; American Geophysical Union: Washington, DC, USA, 2003.
9. Lelieveld, J.; Crutzen, P.J.; Dentener, F.J. Changing concentration, lifetime and climate forcing of atmospheric methane. *Tellus B* **1998**, *50*, 128–150.
10. Birkedal, K.A.; Ersland, G.; Husebø, J.; Kvamme, B.; Graue, A. Geomechanical stability during CH₄ production from hydrates—Depressurization or CO₂ sequestration with CO₂-CH₄ exchange. In Proceedings of the 44th U.S. Rock Mechanics Symposium and 5th U.S.-Canada Rock Mechanics Symposium, Salt Lake City, UT, USA, 27–30 June 2010.
11. Espinoza, D.N.; Santamarina, J.C. P-wave monitoring of hydrate-bearing sand during CH₄-CO₂ replacement. *Int. J. Greenh. Gas Control* **2011**, *5*, 1031–1038.
12. Tohidi, B.; Yang, J. CO₂ hydrates could provide secondary safety factor in subsurface sequestration of CO₂. *Environ. Sci. Technol.* **2010**, *44*, 1509–1514.
13. Ballard, A.L.; Sloan, E.D., Jr. The next generation of hydrate prediction: An overview. *J. Supramol. Chem.* **2002**, *2*, 385–392.
14. Lee, H.; Seo, Y.; Seo, Y.-T.; Moudrakovski, I.L.; Ripmeester, J.A. Recovering methane from solid methane hydrate with carbon dioxide. *Angew. Chem.* **2003**, *115*, 5202–5205.
15. Lee, H.; Seo, Y.; Seo, Y.-T.; Kim, D.Y.; Moudrakovski, I.L.; Ripmeester, J.A.; Sang-Eon Park, J.-S.C.; Kyu-Wan, L. Replacement of methane hydrate by carbon dioxide: ¹³C NMR study for studying a limit to the degree of substitution. In *Studies in Surface Science and Catalysis*; Elsevier: Amsterdam, The Netherlands, 2004; Volume 153; pp. 495–500.

16. Park, Y.; Cha, M.; Cha, J.H.; Shin, K.; Lee, H.; Park, K.P.; Huh, D.G.; Lee, H.Y.; Kim, S.J.; Lee, J. Swapping carbon dioxide for complex gas hydrate structures. In Proceedings of the 6th International Conference on Gas Hydrates, Vancouver, BC, Canada, 6–10 July 2008; p. 6.
17. Ota, M.; Morohashi, K.; Abe, Y.; Watanabe, M.; Smith, J.R.L.; Inomata, H. Replacement of CH₄ in the hydrate by use of liquid CO₂. *Energy Convers. Manag.* **2005**, *46*, 1680–1691.
18. Graue, A.; Kvamme, B.; Baldwin, B.; Stevens, J.; Howard, J.J.; Aspenes, E.; Ersland, G.; Husebo, J.; Zornes, D. Mri visualization of spontaneous methane production from hydrates in sandstone core plugs when exposed to CO₂. *SPE J.* **2008**, *13*, 146–152.
19. Kvamme, B.; Graue, A.; Buanes, T.; Kuznetsova, T.; Ersland, G. Storage of CO₂ in natural gas hydrate reservoirs and the effect of hydrate as an extra sealing in cold aquifers. *Int. J. Greenh. Gas Control* **2007**, *1*, 236–246.
20. Yuan, Q.; Sun, C.-Y.; Liu, B.; Wang, X.; Ma, Z.-W.; Ma, Q.-L.; Yang, L.-Y.; Chen, G.-J.; Li, Q.-P.; Li, S.; *et al.* Methane recovery from natural gas hydrate in porous sediment using pressurized liquid CO₂. *Energy Convers. Manag.* **2013**, *67*, 257–264.
21. Hester, K.C.; Stevens, J.C.; Howard, J.J. Composition studies to determine rate and extent of CO₂ exchange in a hydrate-bearing core. In Proceedings of the 7th International Conference on Gas Hydrates, Edinburgh, UK, 17–21 July 2011.
22. Ersland, G.; Husebø, J.; Graue, A.; Baldwin, B.A.; Howard, J.; Stevens, J. Measuring gas hydrate formation and exchange with CO₂ in bentheim sandstone using mri tomography. *Chem. Eng. J.* **2010**, *158*, 25–31.
23. Deusner, C.; Bigalke, N.; Kossel, E.; Haeckel, M. Methane production from gas hydrate deposits through injection of supercritical CO₂. *Energies* **2012**, *5*, 2112–2140.
24. Liu, B.; Pan, H.; Wang, X.; Li, F.; Sun, C.; Chen, G. Evaluation of different CH₄-CO₂ replacement processes in hydrate-bearing sediments by measuring P-wave velocity. *Energies* **2013**, *6*, 6242–6254.
25. Phale, H.A.; Zhu, T.; White, M.D.; McGrail, B.P. Simulation study on injection of CO₂-microemulsion for methane recovery from gas-hydrate reservoirs. In *SPE Gas Technology Symposium*; Society of Petroleum Engineers: Calgary, AL, Canada, 2006.
26. White, M.D.; Wurstner, S.K.; McGrail, B.P. Numerical studies of methane production from class 1 gas hydrate accumulations enhanced with carbon dioxide injection. *Mar. Pet. Geol.* **2011**, *28*, 546–560.
27. Schoderbek, D.; Boswell, R. Ignik sikumi #1, gas hydrate test well, successfully installed on the alaska north slope. *Fire Ice* **2011**, *11*, 1–5.
28. Parshall, J. Production method for methane hydrate sees scientific success. *J. Pet. Technol.* **2012**, *64*, 50–51.
29. Thomas, W.J.; Adams, M.J. Measurement of the diffusion coefficients of carbon dioxide and nitrous oxide in water and aqueous solutions of glycerol. *Trans. Faraday Soc.* **1965**, *61*, 668–673.
30. Demurov, A.; Radhakrishnan, R.; Trout, B.L. Computations of diffusivities in ice and CO₂ clathrate hydrates via molecular dynamics and monte carlo simulations. *J. Chem. Phys.* **2002**, *116*, 702–709.

31. Davies, S.R.; Lachance, J.W.; Sloan, E.D.; Koh, C.A. A novel approach to measuring methane diffusivity through a hydrate film using differential scanning calorimetry. In Proceedings of the 6th International Conference on Gas Hydrates, Vancouver, BC, Canada, 6–10 July 2008.
32. Husebø, J. *Monitoring Depressurization and CO₂-CH₄ Exchange Production Scenarios for Natural Gas Hydrates*; University of Bergen: Bergen, Norway, 2008.
33. Birkedal, K.A. *Empirical and Numerical Evaluation of Mechanisms in Gas Production from CH₄-hydrates: Emphasis on Kinetics, Electrical Resistivity, Depressurization and CO₂-CH₄ Exchange*; University of Bergen: Bergen, Norway, 2013.
34. Circone, S.; Kirby, S.; Stern, L.A. Direct measurement of methane hydrate composition along the hydrate equilibrium boundary. *J. Phys. Chem.* **2005**, *109*, 9468–9475.
35. Petrich, C.; Eicken, H. Growth, structure and properties of sea ice. In *Sea Ice*; Wiley-Blackwell: Hoboken, NJ, USA, 2010; pp. 23–77.
36. Duan, Z.; Sun, R. An improved model calculating CO₂ solubility in pure water and aqueous NaCl solutions from 273 to 533 K and from 0 to 2000 bar. *Chem. Geol.* **2003**, *193*, 257–271.
37. Collett, T.S.; Boswell, R.; Lee, M.W.; Andersen, J.L.; Rose, K.; Lewis, K.A. Evaluation of long-term gas-hydrate-production testing locations on the Alaska North Slope. *SPE Reserv. Eval. Eng.* **2012**, *15*, 243–264.
38. Schoderbek, D.; Martin, K.L.; Howard, J.; Silpngarmert, S.; Hester, K.C. North slope hydrate field trial: CO₂/CH₄ exchange. In Proceedings of the Arctic Technology Conference, Houston, TX, USA, 3–5 December 2012.
39. Kneafsey, T.J.; Nakagawa, S.; Borglin, S.E. *Properties of Hydrate-bearing Sediments Subjected to Changing Gas Compositions*; Lawrence Berkeley National Laboratory: Berkeley, CA, USA, 2013.

© 2015 by the authors; licensee MDPI, Basel, Switzerland. This article is an open access article distributed under the terms and conditions of the Creative Commons Attribution license (<http://creativecommons.org/licenses/by/4.0/>).